Materials Today Communications 39 (2024) 109016

Contents lists available at ScienceDirect

Materials Today Communications

journal homepage: www.elsevier.com/locate/mtcomm

A data-driven approach to model the martensitic transformation temperature in strain-induced metastable austenitic steels

Abhishek Kumar Thakur [a,b], Bhaskarjyoti Das [b,c], Sandip Ghosh Chowdhury [b,*]

[a] Department of Materials Science and Engineering, University of Arizona, Tucson, AZ 85721, United States of America
[b] Materials Engineering Division, CSIR – National Metallurgical Laboratory, Jamshedpur 831007, India
[c] Department of Metallurgy and Materials Engineering, Indian Institute of Engineering Science and Technology, Shibpur, Howrah, West Bengal 711103, India

ARTICLE INFO

Keywords:
Deformation-induced transformation
Martensite transformation temperature
Predictive modelling
Steel database
Machine learning

ABSTRACT

Strain-induced metastable austenitic stainless steels form an important class of materials in metallurgical industries for their wide range of applications. These steels undergo austenite-martensite phase transformation at temperatures above martensite start temperature, M_s, at which martensite is formed on mechanical deformation, also known as the M_d temperature. M_d temperature depends on several factors related to the steel and is important from alloy design perspective. In the literature, there are quite a few equations based on composition of the steels for the prediction of M_d temperature. However, it is well known that the transformation from austenite to martensite is dependent on the austenite grain size as well as deformation conditions i.e. strain, strain rate and temperature of deformation. In the present work, the role of those parameters has also been considered. The model is implemented using fourteen input parameters viz., composition, grain size, amount of strain, temperature of deformation, and strain rate. The architecture of the neural network model is optimized rigorously to predict the M_d temperature on a par with actual value. It has been shown that grain size and strain rate have very negligible influence whereas strain and temperature of deformation have quite strong role. M_d temperature is increased with increasing strain whereas the temperature of deformation shows opposite dependence on it. An empirical equation thus, has been established to calculate the M_d temperature of a steel as a function of its composition, grain size, temperature of deformation and strain. The final optimized model is then deployed to predict the M_d temperature of different steels and predictions are found to be in close agreement to the experimentally measured M_d temperatures. The developed model is general and can be extended to include other parameters as well as various other steel alloys.

1. Introduction

Austenitic stainless steels form an important class of engineering materials due to their good corrosion resistance and mechanical properties. The strength/elongation ratio in austenitic steels can be adjusted within a wide range using mechanical deformation depending on its application design requirements. The austenite phase in these steels is metastable and can transform into a martensite phase at a temperature that is well above the martensite start temperature, M_s. The maximum temperature at which deformation-induced martensitic transformation can take place is known as the M_d temperature. This deformation-induced austenite to martensite transformation depends on the characteristics of steel such as its composition, austenitic grain size, deformation temperature, and strain [1].

The M_d temperature of metastable austenitic stainless steel is an important alloy design parameter that is beneficial in providing a required combination of strength and ductility. It is broadly governed by the stability of the austenite phase and hence all the parameters that affect the austenite phase stability. The presence of C and Mn in steel drastically affects its M_d temperature. This is because both C and Mn are austenite phase stabilizers i.e., it enhances the range of temperature over which austenite phase does not transform to martensite. Consequently, the M_d temperature of the steel lowers and hence allows it to be ductile over a large range of temperatures. Similarly, N also stabilizes the austenite phase and helps in lowering the M_d temperature of steel. The effect of C and N on the M_d temperature is thought to be identical [2,3], but it has further been shown that the effect of C is comparatively more significant than N [4]. The presence of other elements such as Cr, Ni, Mo,

* Corresponding author.
E-mail address: sgc@nmlindia.org (S.G. Chowdhury).

https://doi.org/10.1016/j.mtcomm.2024.109016
Received 14 February 2024; Received in revised form 19 April 2024; Accepted 23 April 2024
Available online 26 April 2024
2352-4928/© 2024 Elsevier Ltd. All rights reserved.

Si, Cu, Nb, and Ti also mechanically stabilizes the austenite phase, but their effect is comparatively low. Angel et. al. [2] established an equation that empirically connects the M_d temperature to the amount of various elements present in the steel alloy. This equation is further modified to include the effect of other elements as well [3,4].

While the presence of different elements affects the M_d temperature of steel, austenitic grain size and processing conditions such as amount of strain, deformation temperature, and strain rate also play a significant role. Since the martensitic transformation is a result of diffusionless shear, it is strongly affected by applied stress. Thus, the M_d temperature can also be altered by the application of strain. The applied strain can result in the formation of defects such as shear bands and dislocations within the austenite matrix that can act as nucleation sites for the martensitic transformation and thus raise the M_s temperature to the M_d temperature [5]. Since the metastable austenitic steels undergo phase transformation during mechanical deformation, the determination of their physical and mechanical properties becomes a necessity for carefully optimizing their processing parameters. Determining the M_d temperature further becomes important to avoid any phase transformation during the secondary processing of steels for the manufacturing of finished products. To this end, we present a data-driven tool to study the effect of different elements and processing conditions on the M_d temperature of metastable austenitic steel.

Among various computational tools, a neural network algorithm is an efficient data-driven tool for predictive modeling and statistical analysis. It has found a tremendous application in the field of materials science, including metals [6,7], semiconductors [8] as well as polymeric materials [9]. This results in a new field called "Materials Informatics" which includes artificial neural networks (ANN) [10,11], and ensemble learning methods like decision trees [12], random forests [13], support vector machine (SVM) [14], and gradient boosting [15], among others. Machine learning techniques have been harnessed previously to predict the M_s temperature of different steel alloys [16–18]. A convolutional neural network approach has been employed in which microstructural images and composition are used to predict the M_s temperature of a medium Mn alloy steel [19]. Using a neural network model, Mirzadeh et. al. [20] modeled the volume fraction of strain-induced martensite formed in cold-worked AISI 304 stainless steels as a function of strain and deformation temperature. However, it does not include the effect of various elements present in the alloy on the volume fraction of strain-induced martensite. Considering the elemental composition, temperature, and strain, Mu et. al. [21] present the implementation of various ensemble machine-learning methods to predict the volume fraction of strain-induced martensite formed in alloy steel. However, their database is limited to AISI 200 series Mn alloyed and AISI 300 series Ni alloyed austenitic stainless steels.

Although significant efforts have been made to model the M_s temperature and the volume fraction of strain-induced martensite, modeling of the M_d temperature has not been reported earlier. In this work, a linear supervised neural network model has been reported for predicting the M_d temperature using material-specific parameters such as composition, austenitic grain size (d), strain (ε_s), deformation temperature (T_d), and strain rate ($\dot{\varepsilon}_s$). We have constructed a rich steel database from the existing literature which includes AISI 304, AISI 306, AISI 201, 204Cu, and TRIP steels. The neural network model is optimized, trained, and tested to efficiently predict the M_d temperature of steel using its parameters. Additionally, an empirical equation for the determination of M_d temperature has been established by implementing the feature importance of different elements present in the steel and its processing conditions.

2. Modeling the M_d temperature

M_d temperature of steel is a function of different parameters such as its composition, grain size, amount of strain to which the steel is subjected to, deformation temperature, and strain rate [22]. It is modeled using a data-driven many-to-one supervised neural network model. The aforementioned parameters about a wide range of steels, which undergo strain-induced martensitic transformation, are collected along with their corresponding M_d temperatures. The collected data is reviewed, cleaned, and subjected to exploratory data analysis to understand the correlation between different parameters as well as the importance of each of the parameters on the M_d temperature. This provides a preliminary data analysis on strong or weak dependence of different elements and other mechanical parameters such as grain size, deformation temperature, and strain on the M_d temperature.

In the next step, the database is normalized and fed into a supervised neural network model for the prediction of M_d temperature. The neural network model is a many-to-one linear model whose architecture is further optimized in the process. The optimized architecture is selected based on the performance criteria of the model i.e., the degree of fitting of the model in predicting the M_d temperatures of different steel alloys. Although, once a neural network is trained it can be used to make frequent predictions of M_d temperatures of new steel samples. The final trained neural network model is then used to make predictions of the M_d temperatures and its performance is quantitatively analysed. Finally, using the trained network model, physical correlations and insights are obtained and an empirical equation for the calculation of M_d temperature has been established. The equation aims to relate the M_d temperature to the composition of different alloying elements present in the steel along with other parameters. A general overview of the workflow is presented in Fig. 1.

2.1. Dataset preparation

The dataset used in this study is prepared from the existing literature encompassing a wide range of steel alloys with varying elemental composition and mechanical processing parameters [1,23–75]. These include AISI 304, AISI 306, AISI 201, 204Cu, and TRIP steels. In the dataset, apart from composition, we also consider the initial austenitic grain size, deformation temperature, strain at which 50 % martensitic transformation occurs, and the applied strain rate. The data has been extensively collected for tensile testing and deformation during metal forming that induces martensitic transformation. Since the strain rates are not always available in the literature, most of the collected data are not considered in this work. This, in turn, leads to a significant reduction in the volume of data that is used in this work. This is followed by data cleaning to ensure that the insufficient entries of data and the errors in the original dataset have been corrected. The final dataset consists of a total of 193 data points which is used in this work for further analysis.

2.1.1. Composition

The composition of different elements present in steel dictates its final properties such as strength, ductility, toughness, etc. For example, the 204Cu austenitic stainless steel has good formability due to the addition of Cu while the addition of Cr and Ni provides corrosion resistance quality to the AISI 304 stainless steels. Thus, the amount of different elements present is of vital importance and is collected for a wide range of steel. As different steels have different elemental compositions, during the data collection process the composition of some of the elements such as N, Ti, and Nb are not reported. In those cases, since the amount of N present in steel is very low, the composition of N is taken as zero. Similarly, the samples in which the composition of Nb and Ti are not found are taken as zero given their small presence in the reported literature.

The composition distribution range for different elements is presented in Table 1. The data count of all the elements included in the dataset has been plotted as a histogram distribution shown in Fig. 2. Although the composition of C ranges to 0.17 most of the collected data has a low presence of carbon. The concentration of Mo and Cu content is mostly limited to less than 1 wt% with a few samples having more than that in the steel composition. The composition of N and Si is limited to

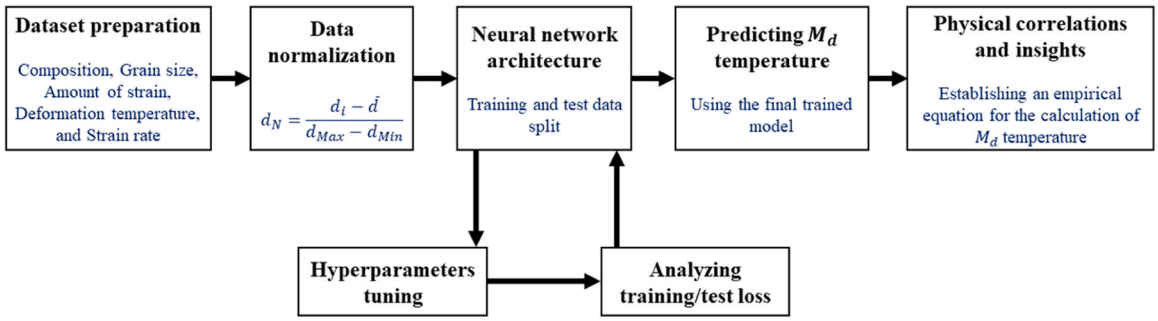

Fig. 1. Schematic flowchart enlisting different stages of this work.

Table 1
Data summary compiled from literature survey. It consists of compositions of various elements, grain size, amount of strain, deformation temperature, strain rate, and M_d temperature.

Parameter	Mean	Standard deviation	Minimum	Maximum
C(wt%)	0.04	0.033	0.001	0.17
Mn(wt%)	2.60	2.60	0.67	17.60
Cr(wt%)	17.16	1.78	0.0	19.08
Ni(wt%)	7.56	2.55	0.0	13.48
Mo(wt%)	0.46	0.82	0.0	4.80
N(wt%)	0.05	0.06	0.0	0.24
Si(wt%)	0.50	0.29	0.2	3.22
Cu(wt%)	0.18	0.38	0.0	3.21
Nb(wt%)	0.003	0.01	0.0	0.09
Ti(wt%)	0.03	0.10	0.0	0.67
d (μm)	32.40	38.68	0.5	285.0
ε_s	44.68	30.45	0.22	166.73
$T_d(^oC)$	-16.09	74.85	-269.0	80.0
$\dot{\varepsilon}_s(s^{-1})$	4.46	24.27	0.0	200.0
$M_d(^oC)$	29.97	32.57	-66.51	221.41

0.25 and 1.2 wt%, respectively. Further, it can be observed that Ni has an extensive range of composition distribution varying from around 2–13 wt%, whereas the distribution of Cr is minimal and is mainly present in the range of 14–19 wt%. Mn content is mostly concentrated between 1 – 2 wt% with a few data points between 6 and 9 wt%.

2.1.2. Grain size, amount of strain, deformation temperature, and strain rate

The dependence of martensite start temperature on grain size, amount of strain, deformation temperature, and strain rate has been studied previously [4,20,76–79]. In general, it is observed that the strain-induced martensite start temperature decreases with a decrease in grain size [80]. However, small grain size mainly in the range 1–100 μm has negligible effect on the martensite formation temperature [76]. The effect of grain size on the M_d temperature is related to the fact that grain boundaries in annealed austenite provide the necessary nucleation ground for martensite formation. The austenite phase is stable at elevated temperatures which is difficult to transform into martensite and thus reduces the martensite formation temperature [79]. However, increasing the amount of strain increases the volume of transformed martensite and thus brings up the martensite start temperature. This is attributed to the fact that with an increase in strain, the formation of shear band accelerates which, in turn, increases the kinetics of strain-induced martensite formation [77]. Formation of shear bands and interaction between them is higher in coarse grains and that also leads to faster kinetics of transformation of austenite to martensite.

The collected data of steels has a wide range of grain size, amount of strain, deformation temperature, and strain rate. The grain size ranges from 0.5 μm to 285 μm as shown in Table 1. The amount of strain varies from 0.22 % to 166.73 %. The collected data samples also show deformation over a wide range of temperatures from -269^oC to 80^oC and to a strain rate of up to $200s^{-1}$.

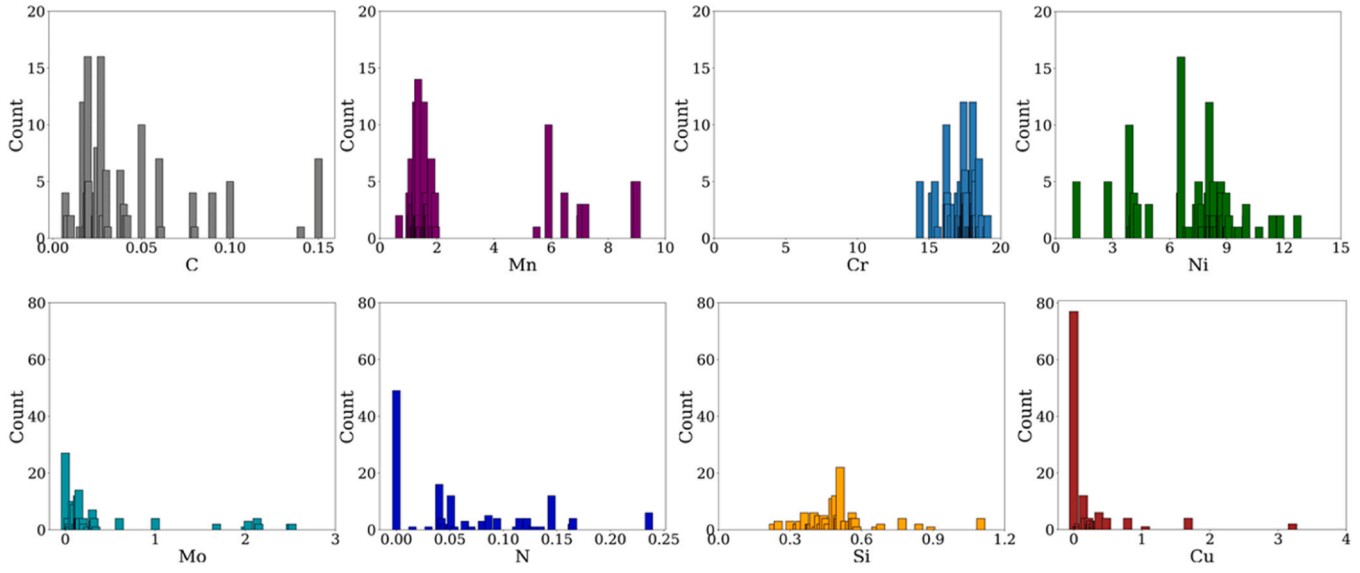

Fig. 2. Histograms showing the composition distribution range with its corresponding number of counts for various elements considered.

2.1.3. M_d temperature

M_d temperature is an important factor from the perspective of alloy design and development. It affects the final properties of steel using strain-induced martensitic transformation from the austenite phase. In contrast to lower austenite stability, higher austenite stability leads to the formation of strain-induced martensite with high strength and ductility [81]. This phenomenon plays a major role in the final product performance and is considered a major criterion (Transformation-induced plasticity, TRIP) for alloy development. Beyond M_d temperature, there will not be any transformation under mechanical deformation.

As previously mentioned, the M_d temperature of steel depends on its elemental composition and different mechanical properties. Several equations relating the M_d temperature of a steel alloy to its elemental composition have been proposed in the literature and are an active area of research. According to Angel [2], the M_d temperature is related to the elemental composition of steel as shown in Eq. (1)

$$Md_{30}(K) = 686 - 462(\%C + \%N) - 9.2\%Si - 8.1\%Mn - 13.7\%Cr - 9.5\%Ni - 18.5\%Mo \quad (1)$$

where Md_{30} is the temperature corresponds to the formation of 50 % martensite by volume at a strain of 0.3 in austenitic stainless steels and all the elements are in weight percentage. The equation is further modified by Nohara et al. [3] by adding the influence of Nb content on M_d temperature as shown in Eq. (2)

$$Md_{30}(^oC) = 551 - 462(\%C + \%N) - 9.2\%Si - 8.1\%Mn - 13.7\%Cr - 29(\%Ni + \%Cu) - 18.5\%Mo - 68\%Nb - 1.42(Gs - 8) \quad (2)$$

where Gs is the ASTM grain size number, and all the elements are in weight percentage. It shows that with decreasing ASTM grain size the M_d temperature of a steel increases.

In both equations, it can be observed that the M_d temperature is strongly dependent on the composition of various elements that are present in the steel. The presence of C and N heavily influences the M_d temperature as compared to other elements as their addition stabilizes the austenite phase and thus depresses the M_d temperature. It can be observed from Eqs. (1) and (2) that the effect of C and N content on the M_d temperature of steel is identical. However, Masumura et. al. [4] presented a modified equation, Eq. (3), in which it is shown that the effect of C content on the M_d temperature is more significant than N. In other words, C stabilizes the austenite phase in steel by depressing the M_d temperature to a greater extent than N.

$$Md_{30}(K) = 800 - 333\sqrt{C_{eq}} - 10.3\%Si - 12.5\%Mn - 10.5\%Cr - 24.0\%Ni - 5.6\%Mo; C_{eq} = \%C + a\%N; a = 0.931 - 0.000281\exp(0.0219T) \quad (3)$$

where C_{eq} represents C equivalent which essentially consists of C and N composition, and T is the temperature.

The effect of other parameters such as the grain size, amount of strain, deformation temperature, and strain rate on the M_d temperature has also been studied extensively. Deformation carried out at elevated temperatures results in stabilizing the austenitic phase present in steel and consequently reduces the M_d temperature [79]. Strain also plays an important part in dictating the M_d temperature and the amount of martensite formed. For instance, with an increase in the strain level, the volume fraction of transformed martensite increases [82]. This is mainly because there is an increase in the formation rate of the shear band with increasing strain which accelerates the kinetics of strain-induced martensite in steel [77]. However, on the contrary, it is observed that the transformation of martensite is suppressed with an increase in the applied strain rate [78].

Thus, it can be seen that the M_d temperature of steel depends on several factors such as the elemental composition, grain size, deformation temperature, and strain effects. This makes it important to consider these parameters and to study their effect on the M_d temperature. For each data point collected, a careful inspection is carried out to include as many parameters as possible available in the literature. In a few cases, the austenitic grain size has not been reported in the literature. For those cases, efforts have been made to measure the grain size from the corresponding reported microstructure in the literature using the linear intercept method. Furthermore, in some work, the M_d temperature is not explicitly mentioned. However, the composition of different elements is reported and thus, the M_d temperature is calculated using an empirical equation for the same from the literature. In the final database, the value of M_d temperature varies from a minimum of -66.51 to a maximum of 221.41^oC.

2.2. Exploratory data analysis

The final database consists of compositions of various elements, grain size, amount of strain, deformation temperature, strain rate, and M_d temperatures of all 193 different steel samples. The detail regarding the compiled database is summarized in Table 1. The collected data of the samples are of low-carbon steels with carbon composition varying from a minimum of 0.001 % to a maximum of 0.17 %. As mentioned earlier, the M_d temperature of the collected data varies between -66.51 and 221.41^oC.

To get insights into the correlation between different pairs of parameters, the dataset is represented using a Pearson correlation matrix in Fig. 3. The diagonal elements represent self-correlation, and thus all the diagonals have a value of one. The off-diagonal terms represent the correlation between different pairs of parameters. It is needless to state that the upper diagonal terms are the same as the lower diagonal terms for correlation between the corresponding pair of parameters. The correlation range varies from -1 to 1. A positive value represents the positive correlation between a pair i.e., an increase in the value of one parameter will likely increase the value of another parameter and vice versa. A zero correlation between a pair means the parameters are not related and a change in one of the parameters will not affect the other parameter. The correlation coefficient between two parameters, p and q, in the dataset can be calculated using Eq. (4)

$$corr_{(pq)} = \frac{1}{n-1} * \frac{\sum_{i=1}^{n}(p_i - \overline{p}) * (q_i - \overline{q})}{\sigma_p * \sigma_q} \quad (4)$$

where n is the total number of data points, i and j varies from 1 to n, p_i and q_i are the i^{th} data point, and $\overline{p}$ and $\overline{q}$ are the mean values of variable p and q with standard deviation σ_p and σ_q respectively.

It is observed from Fig. 3 that C and N are strongly negatively correlated to the M_d temperature i.e., an increase in C or N content will likely reduce the M_d temperature of the steel. In other words, the addition of C and N stabilizes the austenite phase in the steel by depressing the M_d temperature. The strong dependence of mechanical stability of austenite phase on C and N content in steel is consistent with the previous findings in the literature [2–4]. Elements such as Cr, Ni, Mo, and Nb also show a negative correlation with M_d temperature of the steel. Mn and Si content in steel shows a slight positive correlation with M_d temperature which is in contrast difference with previous findings in the literature [2–4]. However, the correlation is not strongly positive and thus can arguably be approximated to be insignificant as compared to other elements. The effect of Cu and Ti content on the M_d temperature of steel is insignificant as the correlation value of these two elements with M_d temperature is very close to zero (Fig. 3). Further, the effect of austenitic grain size on the M_d temperature is also very weak. According to Matsuoka et al., the M_d temperature of a Fe-16 %Cr-10 %Ni alloy is not affected when the austenitic grain size is between 1 and 100 μm [76]. From Table 1, the maximum grain size of the collected sample is 285 μm. However, most of the samples have grain sizes smaller than

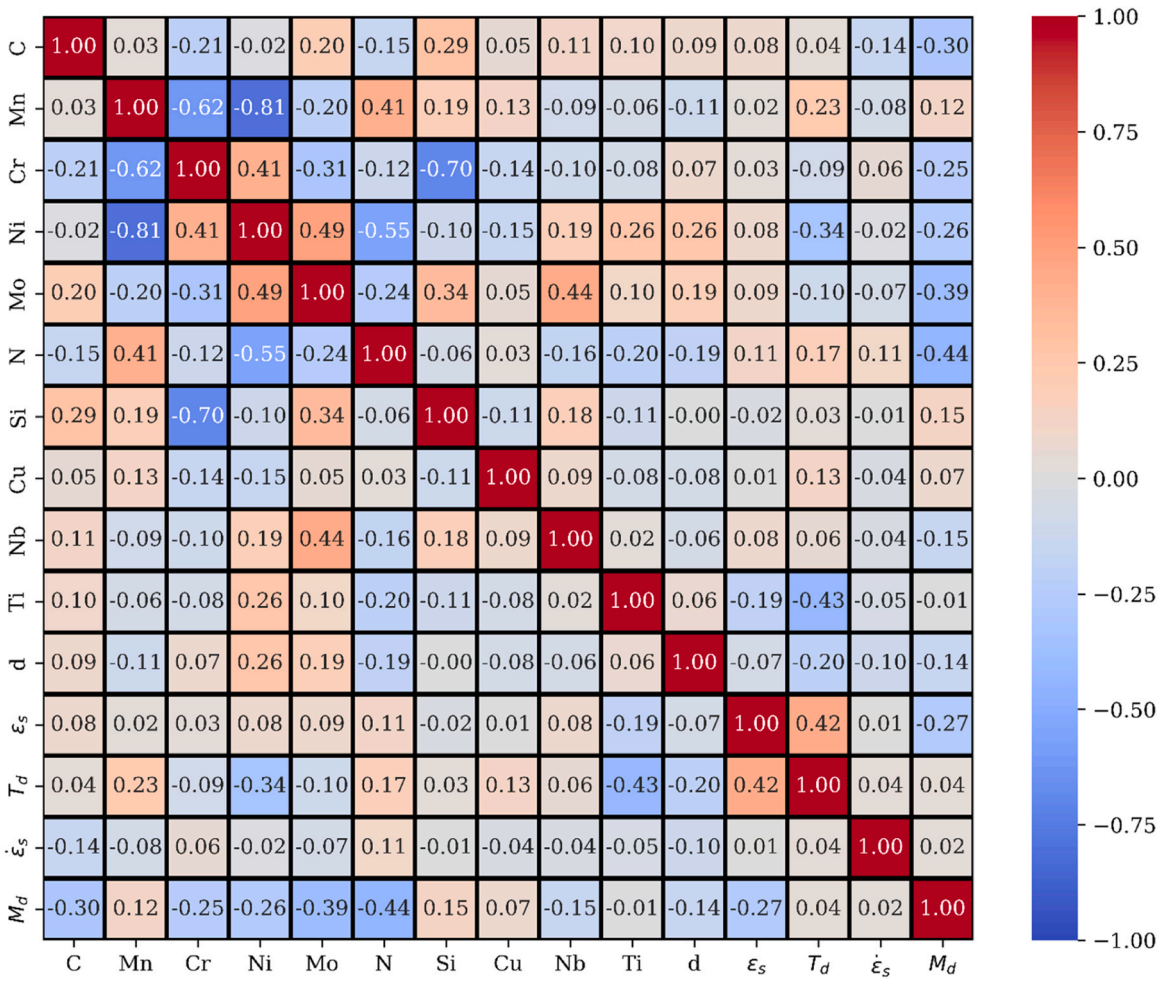

Fig. 3. A Pearson correlation matrix showing the correlation between different pairs of parameters.

100 μm, and only 7 out of 193 samples have grain sizes greater than 100 μm. This explains the observed weak correlation between austenitic grain size and M_d temperature in Fig. 3. Finally, it is observed that the M_d temperature is negatively correlated with the amount of strain and is not significantly correlated with the deformation temperature and strain rate. On the contrary, it has been previously reported that with an increase in the strain amplitude, the amount of deformation-induced martensite also increases [82]. The observation of the correlation of strain with M_d temperature from Fig. 3 is mainly due to the small size of the database and the scarcity of data in the literature.

To further explore the interdependence of different parameters, the compiled database has been represented with pair plots using the seaborn visualization library [83] in Fig. 4. From Fig. 4(a) and (b), it can be observed that low C and N content affects the M_d temperature of steels more significantly when compared to higher concentrations of the same. This is consistent with the findings of Masumura et. al. [84] in which the C and N show a significant effect on the M_d temperature when their concentration is less than 0.1 %. Elements such as Mn, Mo, Si, Cu, Nb, and Ti also affect the M_d temperature when their concentrations are low. On the other hand, the M_d temperature is affected by the higher concentrations of Cr and Ni in the steel. Further, smaller austenitic grain size affects the M_d temperature more when compared to the larger austenitic grain size as is evident from Fig. 4(c). A large range of the amount of strain and deformation temperature also affects the M_d temperature.

2.3. Supervised neural network model

The database is randomly divided into around 80 % and 20 % for training and test datasets respectively. The training dataset consists of 153 data points whereas the test dataset consists of 40 data points. Further details regarding these datasets such as mean, standard deviation, minimum, and maximum values are provided in the supplementary information as Table 1 and 2 for training and test datasets respectively.

2.3.1. Data normalization

Since the present work involves multi-dimensional data and the range of these are significantly different, data normalization becomes important. It is crucial to pass the collected data from a normalization filter to bring the range of all the data to a common platform. This results in weighing off the dominance of any largely positive or largely negative data in the dataset. It also helps the system converge to the global minima during neural network training. The data is normalized using Eq. (5)

$$d_N = \frac{d_i - d_{\min}}{d_{\max} - d_{\min}} \tag{5}$$

where d_N is the normalized data, d_i is the i^{th} data in the database, and $d_{\min}$ and $d_{\max}$ are the minimum and maximum data in the database respectively. Using Eq. (5), all the data will be normalized in the range [0,1]. This normalized data is then fed into the neural network for training and testing purposes. Further, output from the neural network will be de-normalized using the inverse of Eq. (5) to bring it to the original scale.

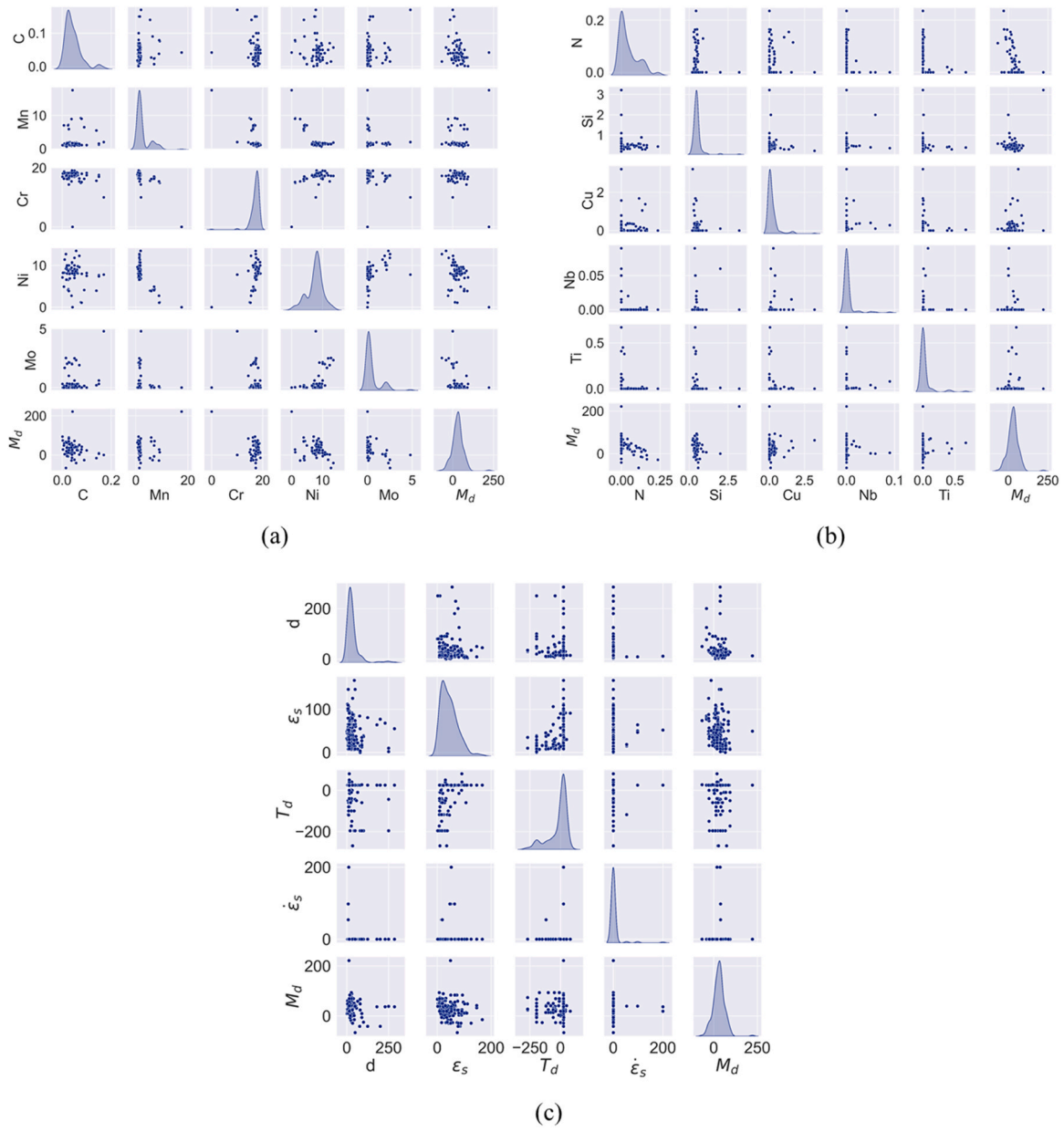

Fig. 4. Pair plot between (a) C, Mn, Cr, Ni, Mo, and M_d, (b) N, Si, Cu, Nb, Ti, and M_d, and (c) d, ε_s, T_d, $\dot{\varepsilon}_s$, and M_d.

2.3.2. *Activation function and Loss calculation*

Since all the data is normalized in the range [0−1], two activation functions viz., Rectified Linear Unit (ReLU) and sigmoid function, are explored for use in the neural network architecture. These two functions are given in Eqs. (6) and (7) and their variation is shown in Fig. 5.

$$ReLU : f(x) = \begin{cases} 0, & x < 0 \\ x, & x \geq 0 \end{cases} \tag{6}$$

$$Sigmoid : f(x) = \frac{1}{1 + e^{-x}}, \quad -\infty < x < \infty \tag{7}$$

Passing all the values in a neural network model to an activation function facilitates the model to learn the multi-dimensional pattern between input parameters and the M_d temperature as the model tries to match the output closely. The choice of activation function(s) depends on the neural network architecture and input values. The ReLU activation makes all the negative input values zero and yields the same value for all positive input values including zero. Thus, the output range of the ReLU activation is [0, ∞]. On the other hand, the sigmoid activation function has a symmetric S-shaped curve around zero with asymptotic behaviour close to 0 and 1 as shown in Fig. 5. Effectively, the sigmoid activation scales all the input values in the range [0,1]. Since the normalized input data is used to train the neural network model, the output range of the data using either ReLU or sigmoid activation function is [0,1].

As explained earlier, fourteen parameters defining steel's characteristics are first normalized and then passed through the input nodes of a supervised neural network model. The output of the network contains just one node and is treated as the normalized M_d temperature. This M_d temperature, calculated from the neural network, will have some expected deviation from the corresponding actual M_d temperature which is collected from the literature. This is due to the generalization nature of the neural network algorithms. The deviation or loss of the calculated M_d temperature should be quantified with respect to the corresponding actual M_d temperature to monitor the performance of the neural network training process. This is carried out using the mean-squared error (MSE) loss given in Eq. (8)

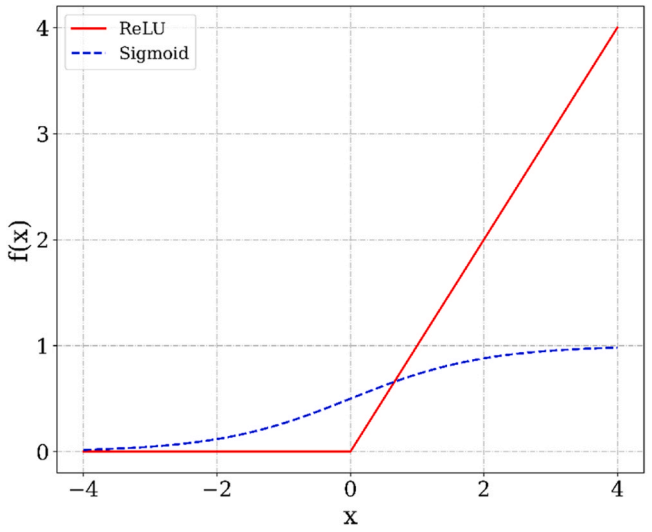

Fig. 5. ReLU and sigmoid activation functions.

$$MSELoss = \frac{1}{n}\sum_{i=1}^{n}\left(y_a - y_p\right)^2 \tag{8}$$

where n is the total number of datapoints, i ranges from 1 to n, y_a is the actual data, and y_p is the predicted data. The MSE loss in the prediction from a neural network is expected to decrease as the number of training cycles increases i.e., as the network learns from the training data. Another metric that is used to quantify the network loss is the mean absolute error (MAE) which is presented in Eq. (9)

$$MAELoss = \frac{1}{n}\sum_{i=1}^{n}\left|y_a - y_p\right| \tag{9}$$

where the symbols have the same meanings as specified above. Both MSE and MAE loss were used during the training and testing to quantify the performance of the neural network models and monitor the outliers. With activation and loss functions defined, the choice of the number of hidden layers and the number of neurons in each of the hidden layers is discussed in the sections below.

2.3.3. One-layered neural network model

Given the fourteen input parameters and one output parameter, a simple neural network model with one hidden layer has been initiated to train the data. Initially, the hidden layer consists of neurons with some random numeric weights that adjust during the training process to best match the actual output. The number of neurons in the hidden layer is not fixed and depends on various parameters such as the number of input and output nodes, amount of data points, and the number of hidden layers. With a smaller number of neurons, the neural network might not be able to map all the data points and thus might not be trained properly. On the other hand, using a lot of neurons in the hidden layer can be computationally expensive and can also result in data overfitting [85]. Thus, the objective here is to find the optimal number of neurons in the hidden layer that yields minimum network loss i.e., MSE and MAE loss. In other words, with the optimal number of neurons in the hidden layer, the difference between the neural network predicted M_d temperature and the actual M_d temperature should be as low as possible. This is performed by systematically varying the number of neurons in the hidden layer from 1 to 20. For each case, the network loss is recorded after training the network to 2000 epochs. Moreover, both activation functions viz., ReLU and sigmoid have been considered on all the values coming after passing through the hidden layer.

Fig. 6(a) and (b) show the variation of MSE and MAE loss with the number of neurons in the hidden layer when ReLU and sigmoid activation functions are used respectively. Using the ReLU activation, as shown in Fig. 6(a), the overall network loss trend shows an increase with the increase in the number of neural nodes present in the hidden layer. The lowest MSE and MAE loss is 0.16 and 0.28, respectively, and is observed when the hidden layer consists of 6 neurons as shown in Fig. 6 (a). In this case, the network seems to be unstable which is also reflected from the uneven loss spikes in the curve.

On the other hand, using the sigmoid activation, the overall network loss shows a decreasing trend with increasing the number of neurons as shown in Fig. 6(b). However, the variation in loss with an increase in the neural nodes is not significant and thus points towards a loss saturation. In this case, the minimum MSE and MAE loss is 0.02 and 0.13, respectively, and is observed when the number of neurons in the hidden layer is 13. Finally, on comparing both cases, it is observed to have a low MSE and MAE loss of the network with 13 neurons in the hidden layer with sigmoid activation function when compared to the network with 6 neurons in the hidden layer with ReLU activation function.

2.3.4. Two-layered neural network model

To further explore the performance of the neural network model, another hidden layer has been added after the first one. To optimize the number of neurons in the second hidden layer, a similar procedure was followed as explained in Section 2.3.3. In the first case, the number of neurons has been fixed to 6 in the first hidden layer, and systematically

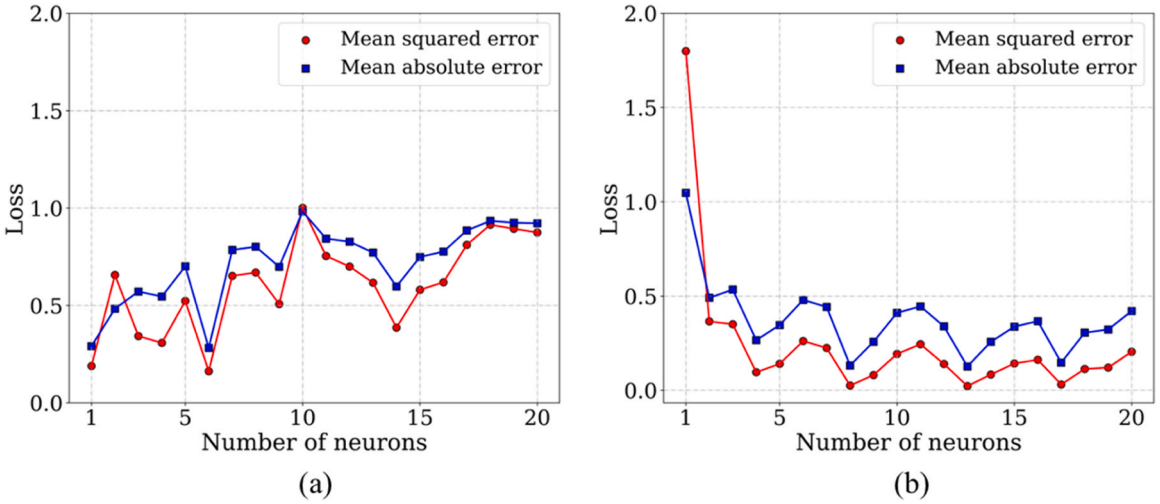

Fig. 6. Training loss variation with number of neurons in a one-layered neural network model using (a) ReLU and (b) sigmoid activation function.

vary the number of neurons from 1 to 20 in the second hidden layer. Further, in this case, ReLU activation has been used in both the hidden layers. Fig. 7(a) shows the mean squared and mean absolute error loss as a function of number of neurons in the second hidden layer. The minimum MSE and MAE loss in this case are 0.09 and 0.24, respectively, and is observed when the number of neurons in the second hidden layer is 17. The overall trend of the network loss decreases with an increase in the number of neurons in the second hidden layer. However, the uneven spikes in the network loss reflect that this neural network state is not very stable.

In the second case, the number of neurons in the first hidden layer has been fixed to 13 and the number of neurons in the second hidden layer has been varied. Sigmoid activation is implemented after both the hidden layers. The variation of network loss with the number of neurons in the second hidden layer in this case is shown in Fig. 7(b). Based on the network loss, the optimal number of neural nodes to consider in the second hidden layer is found to be 7 with the corresponding MSE and MAE loss are 0.19 and 0.35, respectively. The network loss in this does not fluctuate much and seems to saturate with the increasing number of neurons in the second hidden layer.

In the last case, the number of neurons in the first and second hidden layers has been fixed to 13 and 7, respectively based on previous findings. Further, different combinations of ReLU and sigmoid activation are applied after the first and second hidden layers. The minimum loss, in this case, is observed when sigmoid activation is applied after the first hidden layer and ReLU activation is applied after the second hidden layer. The corresponding minimum MSE and MAE loss are 0.20 and 0.38, respectively. Fig. 7(c) shows the variation of network loss as a function of number of neurons in the second hidden layer. In this case, the network is stable with a smaller fluctuation in the loss as a function of the number of neurons.

The optimized neural network architecture consists of an input, two hidden, and an output layer. The input layer consists of 14 neurons to take the parameters that characterize different steel. The first hidden layer consists of 13 neurons followed by a sigmoid activation function. The second hidden layer consists of 7 neurons followed by a ReLU activation. The final output will be collected at the output node providing M_d temperature of the steel. The schematic architecture of the optimized neural network is shown in Fig. 8. Given the small size of the dataset with only 193 total data points, increasing the number of hidden layers might not be beneficial and can lead to data overfitting. Moreover, a shallow neural network is preferred over a deep neural network in the case of a small dataset [86].

2.3.5. *Optimizing learning rate*

Learning is an important parameter of a neural network model that determines the rate at which the model will attain the optimized weights of the neurons. The training of the neural network model starts with some random numerical weights assigned to each neuron in both the hidden layers. As the training progresses, the model tries to match the predicted M_d temperature with the actual M_d temperature and quantifies it using Eqs. (10) and (11). After each epoch, the model adjusts the weights assigned to different neurons in such a way that the error is as low as possible. For this procedure, it uses a well-known gradient descent algorithm [87] which is expressed mathematically in Eq. (10).

$$w_{new} = w_{old} - \alpha \frac{dL}{dw_{old}} \tag{10}$$

where w_{old} and w_{new} are the old weights and new weights of the neurons in the hidden layer, L is the loss function, and α is the learning rate. A large value of α can lead to a situation in which there is a drastic change in the weights of the neurons. In this condition, the neural network model can skip the optimal weights of the neurons. On the other hand, a small value of α will require the neural network to perform many iterations so that the weights of neurons will converge to optimal values. Thus, defining the α of a neural network model is an optimization process that is critical for its performance.

To optimize the α, the performance of the neural network model was recorded by systematically varying the α. The performance of the model, in terms of mean squared and mean absolute error is presented in Fig. 9 as a function of α. It can be observed from Fig. 9 that with an increase in learning rate, the MSE as well as MAE loss of the neural network rises significantly. This explains the condition where the weights of the neurons in the neural network model change drastically, and the model is not able to find the optimal set for the same. At lower values of α, the network loss is significantly low. The lowest value of MSE and MAE is 0.03 and 0.14 which is obtained when the α is set to 0.001. Although, an adaptive learning rate can also be implemented in training a neural network model which changes as the training progresses, in this work the learning rate has been fixed to 0.001.

3. Results and discussion

The final neural network architecture implemented in the prediction of M_d temperature contains 14 input nodes, and two hidden layers with the first hidden layer containing 13 neurons followed by sigmoid activation and the second hidden layer containing 7 neurons followed by ReLU activation, 1 output neuron, and a learning rate of 0.001. It is implemented using a simple regression-based linear neural network model written in Python using the PyTorch framework [88]. Seaborn [83] and Matplotlib [89] computer software packages are used for plotting and visualization.

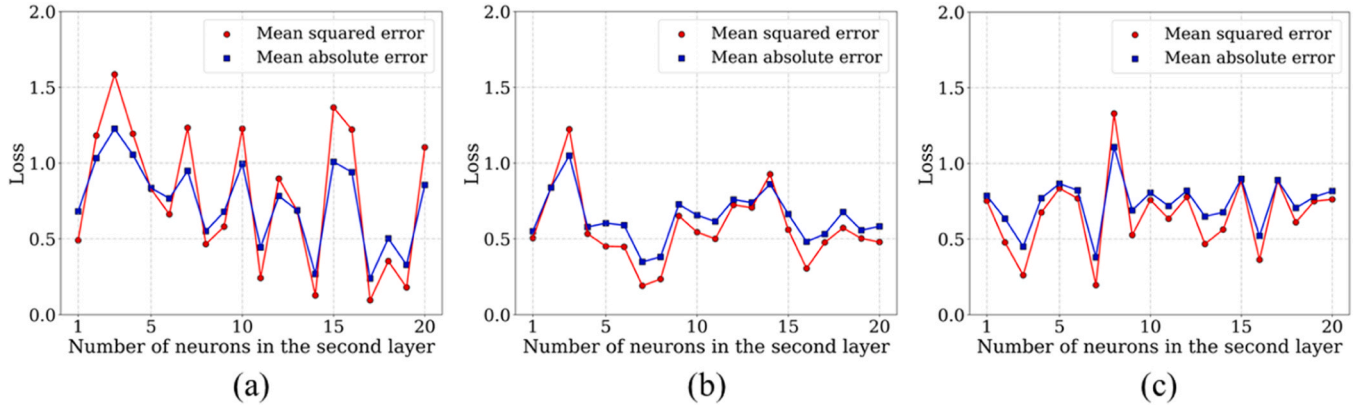

Fig. 7. Training loss variation with the number of neurons in a two-layered neural network model using (a) ReLU activation in both hidden layers, (b) Sigmoid activation in both hidden layers, and (c) Sigmoid in the first and ReLU in the second hidden layer.

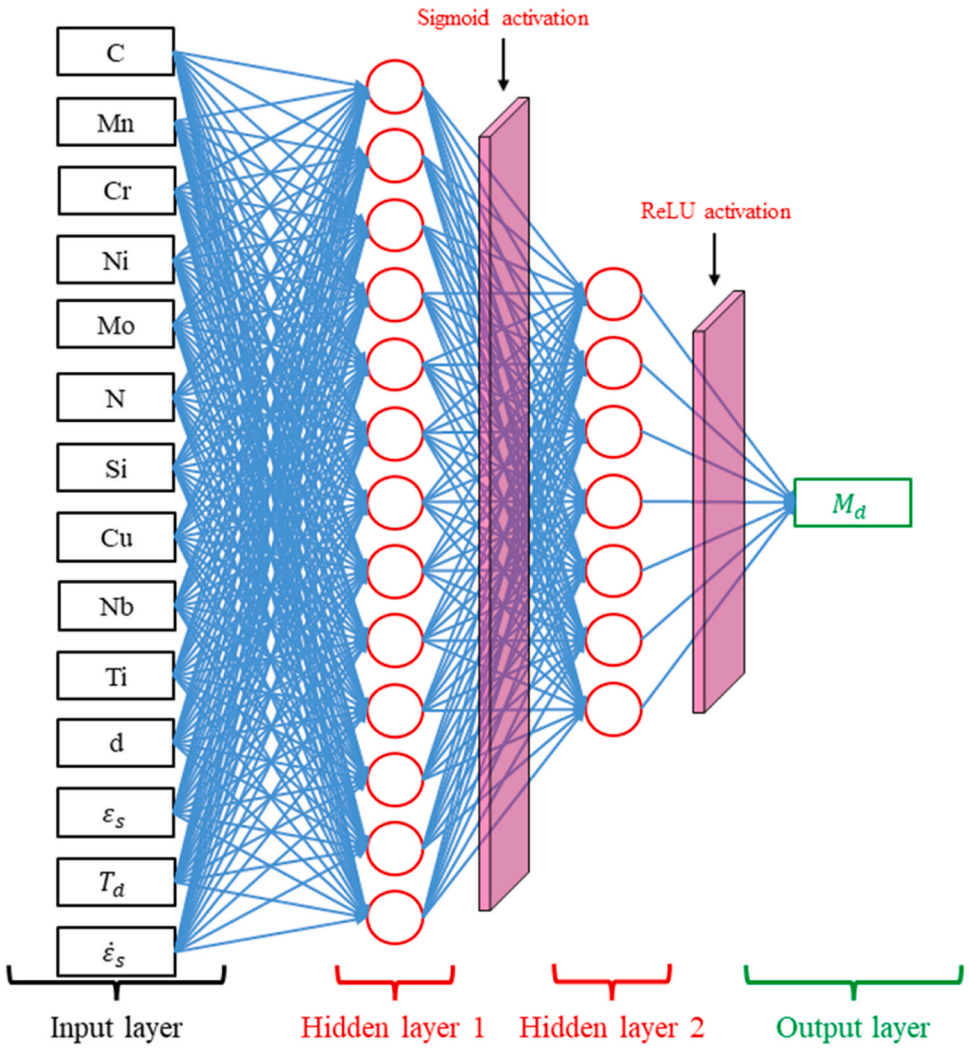

Fig. 8. Neural network architecture with fourteen input neurons, thirteen neurons in the first hidden layer, seven neurons in the second hidden layer, and one output neuron.

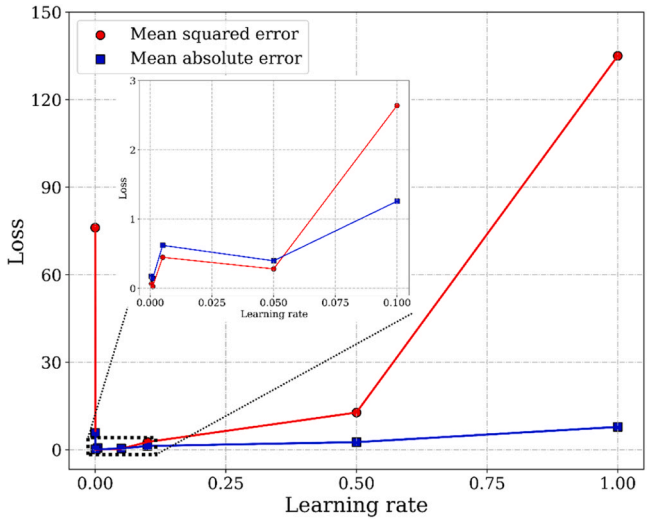

Fig. 9. The variation of mean squared and mean absolute error of the neural network model with different learning rates.

3.1. Model training

The final optimized neural network model shown in Fig. 8 is trained for ten thousand epochs using the training dataset. The trained model after each epoch is used to evaluate its performance on the test dataset. The training and test performance of the model is measured in terms of MSE loss on both datasets. The variation of MSE loss as a function of epochs is shown in Fig. 10 for the first five thousand epochs. Since the training starts with random weights assigned to each neuron in both the hidden layers, the initial loss of the neural network is large. It can be observed that the training, as well as the test loss, decreases with increasing number of epochs. This represents that the neural network model is trained from the input parameters to predict the M_d temperature close to the actual M_d temperature with each epoch. The training test loss of the network after ten thousand epochs is 4.14×10^{-5} and 3.56×10^{-5} respectively which is reasonably good. It is worth noting that at this point both the actual and predicted M_d temperature is normalized. It should be denormalized further using the inverse of Eq. (3) to have a meaningful comparison between the actual and predicted M_d temperatures.

3.2. Performance evaluation

The state of the trained model after ten thousand epochs is then used

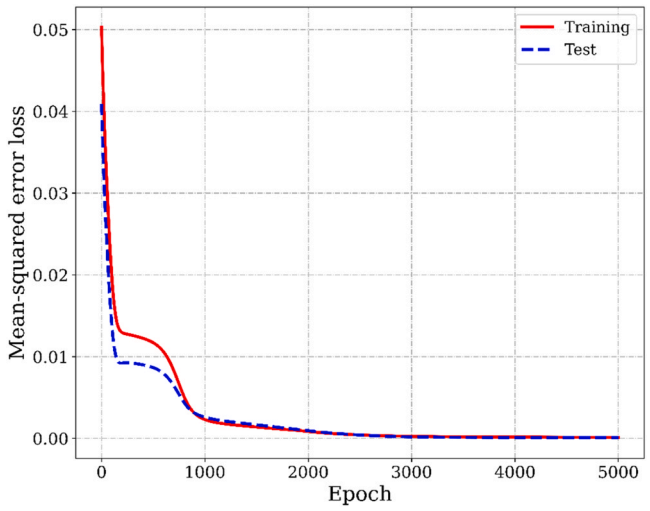

Fig. 10. Training and test loss curve of the final neural network as a function of epoch for the first 5000 epochs.

for the prediction of M_d temperature using the input parameters of the training as well as the test dataset. The accuracy of the trained model is evaluated by comparing the true M_d temperature and the model-predicted M_d temperature after denormalization as shown in Fig. 11. Each dot represents the actual M_d temperature of a steel and its corresponding neural network predicted M_d temperature. The figures show an ideal line (in solid blue) with slope 1 and the data (represented by the dots) falling on this line will have an accurate prediction for the M_d temperature. However, since the neural network is a generalization algorithm, there is an expected departure of the predicted M_d temperature from the corresponding actual M_d temperature. Fig. 11(a) and (b) show the actual and the corresponding predicted M_d temperatures for training and test datasets, respectively. Although not ideal, most of the values fall along the ideal line shows the neural network is well trained and can make acceptable predictions. Moreover, a linear fit of the training and test data prediction provides a slope of 0.99 and 0.98, respectively which is very close to the ideal line. This further reinforces the performance of the trained neural network model and its applicability to predict the M_d temperature of different steel samples to a reasonable accuracy.

Fig. 12(a) and (b) show the error in the predicted M_d temperature with respect to the actual M_d temperature using a bar plot for all the samples in training and test datasets, respectively. It can be observed that for both training and test datasets, the error in M_d temperature predictions can either be positive or negative. From Table 1 it can be observed that the M_d temperature varies in the range [-66.51^oC, 221.41^oC] in the initial database. For the training dataset, the error in the predicted M_d temperatures with respect to their corresponding actual M_d temperatures are in the range [-7.22^oC, 6.64^oC]. For the test dataset, this error is in the range [-6.04^oC, 4.27^oC]. This shows that the model prediction of the M_d temperatures is in good agreement with the corresponding actual M_d temperatures.

3.3. Neural network generated equation and its physical interpretation

As explained earlier, the final M_d temperature depends on several parameters related to the corresponding steel composition. Thus, efforts have been made to establish an empirical equation that relates the M_d temperature of steel to its parameters using the final trained neural network model. Since the final M_d temperature is a function of 14 input parameters, the corresponding weights of these nodes present in the neural network model are used to calculate their corresponding coefficients. This further provides us with an idea of feature importance and their effect on the M_d temperature. In general, the feature importance of each input parameter is calculated by measuring the change in the network prediction error against a given change in the feature value [66]. The features which drastically affect the network's error are considered relatively more significant than others. On the contrary, a feature is supposed to be less significant if it does not reflect a drastic change in the network prediction error on changing its value.

The calculated empirical equation from the trained neural network using the mean impact value is shown in Eq. (11)

$$M_d(^oC) = 412 - 462[\%C + \%N] - 9.2\%Si - 8.0\%Mn - 13.7\%Cr - 9.5\%Ni - 0.15\%Cu - 18.65\%Mo + 0.01d - 0.0067(T_d - \varepsilon_s) \quad (11)$$

It is evident from the coefficients of different elements in Eq. (11) that the composition of C and N in the steel strongly affects the M_d temperature. They are followed by the importance of the rest of the elemental composition present in the steel. The grain size has a weak influence on the M_d temperature. Also, mechanical processing conditions such as the temperature of deformation, strain, and strain rate have almost negligible influence on the M_d temperature. This equation has no coefficient for strain rate, which implies that the strain rate does not play any role in deciding the M_d temperature.

The calculated empirical equation, Eq. (11), from the trained neural network model, is similar to the equations provided by Angel and Nohara et. al. as shown in Eqs. (1) and (2) respectively. The coefficients

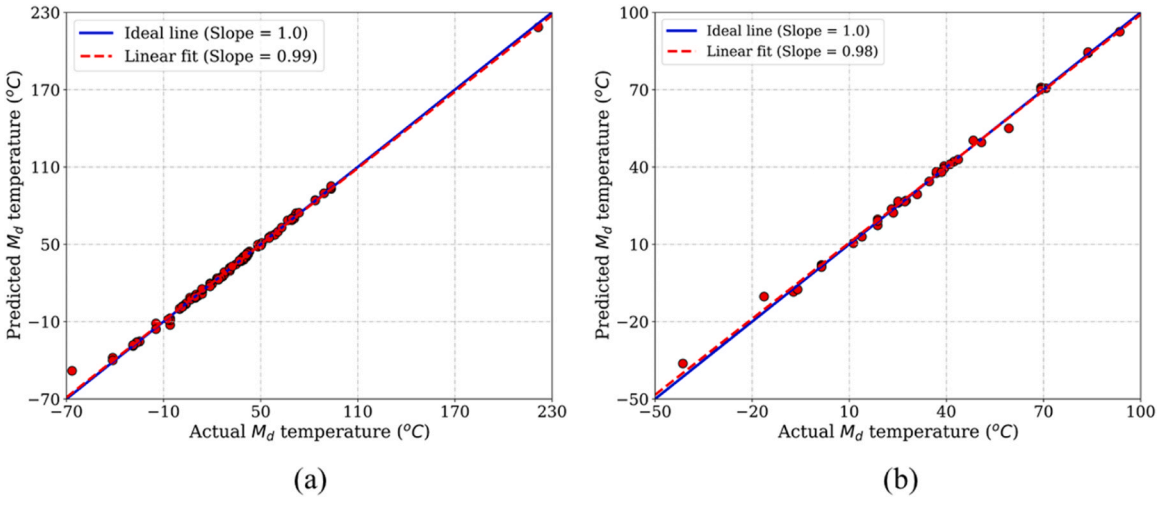

Fig. 11. Comparison between the actual and predicted M_d temperatures of different steel samples in (a) training and (b) test dataset.

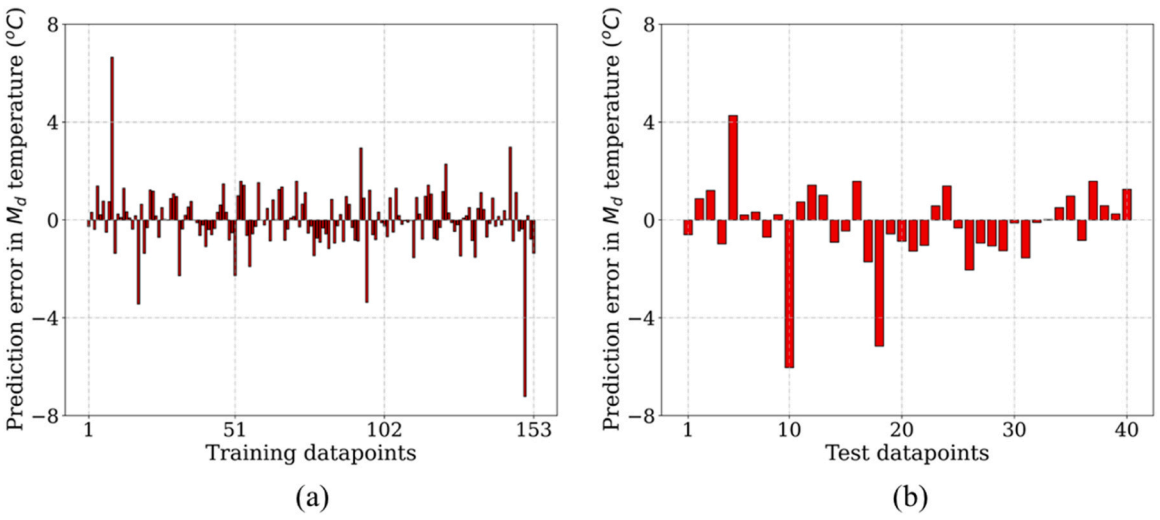

Fig. 12. The prediction error in the M_d temperature for samples in (a) training and (b) test dataset.

of the composition of C, N, Si, and Cr are strikingly common in these three equations with a very small change in the coefficient of Mn. The predicted coefficient of Mo concentration in Eq. (11) is more negative as compared to the same in Eqs. (1) and (2). This mainly points towards the fact that Mo is a bit more influential in stabilizing the austenite phase and thus comparatively depresses the M_d temperature more effectively. Similarly, the predicted coefficients of Ni and Cu concentrations in Eq. (11) are less when compared to Eq. (2). Thus, although Ni and Cu are austenite phase stabilizers, their influence on stabilizing the austenite phase is relatively less when comparing the same from the equations provided in the literature. In other words, according to the trained neural network model, Ni and Cu reduce the M_d temperature to a lesser extent than reported previously in the literature. This is probably because of the little presence of Cu in the class of strain-induced metastable austenitic stainless steels.

Further, although previous works dictate the effect of austenitic grain size, temperature of deformation, and strain, the neural network model shows no significant effect of the same on the M_d temperature of steel. Mathematically, it can be inferred that an increase in the grain size increases the M_d temperature because of its small positive coefficient in Eq. (11). It can be physically correlated to the fact that an increase in the prior austenitic grain size, or decrease in grain boundary area, promotes diffusion-less martensitic transformation. Järvenpää et al. [90] and Maréchal [91] observed a continuous increase in the transformation rate with an increase in grain size up to 24 μm. It indirectly infers that M_d temperature increases with grain size. Saeed-Akbari et al. [92] and Somani et al. [93] observed similar behaviour and it is observed that for finer grains, stacking fault energy (SFE) of the steel is quite higher in comparison to the coarser grains and that is why the tendency for transformation to martensite is reduced. This, in turn, says that coarser grains lead to a higher propensity to martensite formation. It is to be noted that in coarser grains formation of shear bands and their intersections are quite higher. A schematic description of the same has been presented by Jain and Varshney [94].

Talonen et al. [95] observed that martensite transformation is suppressed with increasing strain rate. It is reported that at a higher strain rate, there is the generation of adiabatic heating which decreases the free energy of the transformation of austenite to martensite [96]. It has also been mentioned that temperature dependence of SFE may restrict the formation of shear bands of critical thickness and that leads to a reduction in transformation rate. Thus, it can be concluded that strain rate does not play any role in controlling the M_d. The temperature of deformation also has negligible impact on the M_d temperature. Amount of strain has observed to increase the M_d temperature; with increasing strain, the amount of defect density increases within the phase and that increases the total free energy of the phase. Due to this, the transformation temperature i.e. temperature at which both austenite and martensite phases become equal increases.

3.4. Summary and conclusion

A neural network framework is developed in this work to predict the M_d temperature of a given steel using its characteristic information such as chemical composition, grain size, amount of strain, deformation temperature, and strain rate. Data from 193 different steel samples with M_d temperature ranging between [-66.51^oC, 221.41^oC] has been collected from several literature sources. A neural network has been created with 14 input nodes for all the characteristic information of the steel and 1 output node for the M_d temperature. The neural network architecture is optimized based on the number of hidden layers, the number of neurons present in each hidden layer, the type of activation function implemented after each hidden layer, and the learning rate. The proposed final optimized neural network architecture consists of 2 hidden layers with 13 and 7 neurons in the first and second hidden layers respectively. Sigmoid and ReLU activation functions are implemented on all the data after the first and second hidden layers respectively. All the data is normalized in the range [0−1], randomly divided into 80 % training and 20 % test, and used to train and test the neural network model.

The developed neural network model can assist in predicting the M_d temperature of different steel samples. The availability of information about the M_d temperature of a steel alloy provides better control towards materials design. The model can serve as an important tool for designing steel alloys focussing on strain-induced martensitic transformation. Future work includes incorporating new advances in the present model such as Long Short-Term Memory (LSTM) [97] neural network and first-principles and CALPHAD-informed multiscale framework [98]. These developments will aid the existing model in predicting the physics-informed microstructure of the steel alloys for different phases and at different stages of alloy transformation. It provides a computationally and cost-effective tool for material design under different processing conditions.

The major findings can be summarized as follows:

- The final optimized neural network architecture consists of 14 nodes in the input layer, and 2 hidden layers in which the first hidden layer consists of 13 neurons followed by a sigmoid activation function

whereas the second hidden layer consists of 7 neurons followed by a ReLU activation function, and 1 node in the output layer.

- An empirical equation has been set up using the trained neural network model to calculate the M_d temperature as a function of elemental composition present in the steel, deformation temperature, and strain. The equation is similar to the equations previously reported in the literature with a minor coefficient change for Mn, Mo, Ni, and Cu.
- The amount of C and N present in the steel influences its M_d temperature to a greater extent as compared to any other element.
- Austenite phase grain size and strain rate are observed to have negligible influence on the M_d temperature.
- Strain imparted has a positive influence on the M_d temperature whereas the temperature of deformation has just the opposite.

Author statement

During the preparation of this work the authors did not use any AI or AI-assisted technologies.

CRediT authorship contribution statement

Sandip Ghosh Chowdhury: Writing – review & editing, Supervision, Project administration, Conceptualization. **Bhaskarjyoti Das:** Methodology, Investigation, Formal analysis, Data curation. **Abhishek Kumar Thakur:** Investigation, Formal analysis, Data curation.

Declaration of Competing Interest

The authors declare that they have no known competing financial interests or personal relationships that could have appeared to influence the work reported in this paper.

Data availability

Data will be made available on request.

Acknowledgment

Authors thank The Director, CSIR - National Metallurgical Laboratory, Jamshedpur, for his kind permission to publish this work.

Appendix A. Supporting information

Supplementary data associated with this article can be found in the online version at doi:10.1016/j.mtcomm.2024.109016.

References

[1] J. Talonen, Effect of strain-induced α'-martensite transformation on mechanical properties of metastable austenitic stainless steels, Aalto University, 2007. ⟨https://aaltodoc.aalto.fi/handle/123456789/2870⟩.
[2] T. Angel, Formation of martensite in austenitic stainless steels effects of deformation, temperature, and composition, J. Iron Steel Inst. 177 (1954).
[3] K. Nohara, Y. Ono, N. Ohashi, Composition and grain size dependencies of strain-induced martensitic transformation in metastable austenitic stainless steels, Res. Lab. Kawasaki Steel Corp. 63 (1977) 772–782, https://doi.org/10.2355/tetsutohagane1955.63.5_772.
[4] T. Masumura, K. Fujino, T. Tsuchiyama, S. Takaki, K. Kimura, Effect of carbon and nitrogen on Md30 in metastable austenitic stainless steel, ISIJ Int. 61 (2021) 546–555, https://doi.org/10.2355/isijinternational.ISIJINT-2020-719.
[5] A. Das, P.C. Chakraborti, S. Tarafder, H.K.D.H. Bhadeshia, Analysis of deformation induced martensitic transformation in stainless steels, Mater. Sci. Technol. 27 (2011) 366–370, https://doi.org/10.1179/026708310×12668415534008.
[6] D. Xue, P.V. Balachandran, J. Hogden, J. Theiler, D. Xue, T. Lookman, Accelerated search for materials with targeted properties by adaptive design, Nat. Commun. 7 (2016) 1–9, https://doi.org/10.1038/ncomms11241.
[7] Y. Liu, T. Zhao, W. Ju, S. Shi, S. Shi, S. Shi, Materials discovery and design using machine learning, J. Mater. 3 (2017) 159–177, https://doi.org/10.1016/j.jmat.2017.08.002.
[8] K.B. Irani, J. Cheng, U.M. Fayyad, Z. Qian, Applying machine learning to semiconductor manufacturing, IEEE Expert. Syst. Their Appl. 8 (1993) 41–47, https://doi.org/10.1109/64.193054.
[9] A. Mannodi-Kanakkithodi, G. Pilania, T.D. Huan, T. Lookman, R. Ramprasad, Machine learning strategy for accelerated design of polymer dielectrics, Sci. Rep. 6 (1) (2016) 10, https://doi.org/10.1038/srep20952.
[10] A.K. Thakur, R.P. Gorrey, V. Jindal, K. Muralidharan, A data-driven approach to approximate the correlation functions in cluster variation method, Model. Simul. Mater. Sci. Eng. 30 (2022) 015001, https://doi.org/10.1088/1361-651X/ac3a16.
[11] S.R. Kalidindi, S.R. Niezgoda, A.A. Salem, Microstructure informatics using higher-order statistics and efficient data-mining protocols, Jom 63 (2011) 34–41, https://doi.org/10.1007/s11837-011-0057-7.
[12] J.R. Quinlan, Induction of decision trees, Mach. Learn. 1 (1986) 81–106, https://doi.org/10.1007/BF00116251.
[13] Y.L. Pavlov, Random forests, Random (2019) 1–122, https://doi.org/10.1201/9780429469275-8.
[14] N.H. Farhat, Photonit neural networks and learning mathines the role of electron-trapping materials, IEEE Expert. Syst. Their Appl. 7 (1992) 63–72, https://doi.org/10.1109/64.163674.
[15] J.H. Friedman, Greedy function approximation: a gradient boosting machine, Ann. Stat. 29 (2001) 1189–1232. ⟨http://www.jstor.org/stable/2699986⟩.
[16] M. Rahaman, W. Mu, J. Odqvist, P. Hedström, Machine learning to predict the martensite start temperature in steels, Metall. Mater. Trans. A 50 (2019) 2081–2091, https://doi.org/10.1007/s11661-019-05170-8.
[17] X. Huang, H. Wang, W. Xue, S. Xiang, H. Huang, L. Meng, G. Ma, A. Ullah, G. Zhang, Study on time-temperature-transformation diagrams of stainless steel using machine-learning approach, Comput. Mater. Sci. 171 (2020) 109282, https://doi.org/10.1016/j.commatsci.2019.109282.
[18] C. Wang, K. Zhu, P. Hedström, Y. Li, W. Xu, A generic and extensible model for the martensite start temperature incorporating thermodynamic data mining and deep learning framework, J. Mater. Sci. Technol. 128 (2022) 31–43, https://doi.org/10.1016/j.jmst.2022.04.014.
[19] Z. Yang, Y. Li, X. Wei, X. Wang, C. Wang, Martensite start temperature prediction through a deep learning strategy using both microstructure images and composition data, Materials (Basel) 16 (2023), https://doi.org/10.3390/ma16030932.
[20] H. Mirzadeh, A. Najafizadeh, ANN modeling of strain-induced martensite and its applications in metastable austenitic stainless steels, J. Alloy. Compd. 476 (2009) 352–355, https://doi.org/10.1016/j.jallcom.2008.08.046.
[21] W. Mu, M. Rahaman, F.L. Rios, J. Odqvist, P. Hedström, Predicting strain-induced martensite in austenitic steels by combining physical modelling and machine learning, Mater. Des. 197 (2021) 109199, https://doi.org/10.1016/j.matdes.2020.109199.
[22] D. Kaoumi, J. Liu, F.L. Paul, Deformation induced martensitic transformation in 304 ss, 2016. https://doi.org/https://scholarcommons.sc.edu/cgi/viewcontent.cgi?article=4815&context=etd.
[23] J. Talonen, H. Hänninen, Formation of shear bands and strain-induced martensite during plastic deformation of metastable austenitic stainless steels, Acta Mater. 55 (2007) 6108–6118, https://doi.org/10.1016/j.actamat.2007.07.015.
[24] T. Suzuki, H. Kojima, K. Suzuki, T. Hashimoto, M. Ichihara, An experimental study of the martensite nucleation and growth in 18/8 stainless steel, Acta Met. 25 (1977) 1151–1162, https://doi.org/10.1016/0001-6160(77)90202-4.
[25] S. Sunil, R. Kapoor, Effect of strain rate on the formation of strain-induced martensite in AISI 304L stainless steel, Metall. Mater. Trans. A Phys. Metall. Mater. Sci. 51 (2020) 5667–5676, https://doi.org/10.1007/s11661-020-05968-x.
[26] S. Sadeghpour, V. Javaheri, A. Kermanpur, J. Kömi, Insight to the influence of ti addition on the straininduced martensitic transformation in a high (About 7 wt%) mn stainless steel, Metals (Basel) 10 (2020), https://doi.org/10.3390/met10050568.
[27] K.K. Spencer, M. Véron, Y. Zhang, J.D. Embury, The strain induced martensite transformation in austenitic stainless steels Part 1 - influence of temperature and strain history, Mater. Sci. Technol. 25 (2009) 7–17, https://doi.org/10.1179/174328408×293603.
[28] K. Spencer, J.D. Embury, K.T. Conlon, M. Véron, Y. Bréchet, Strengthening via the formation of strain-induced martensite in stainless steels, Mater. Sci. Eng. A 387–389 (2004) 873–881, https://doi.org/10.1016/j.msea.2003.11.084.
[29] I.R. Souza Filho, M.J.R. Sandim, R. Cohen, L.C.C.M. Nagamine, H.R.Z. Sandim, D. Raabe, Magnetic properties of a 17.6 Mn-TRIP steel: Study of strain-induced martensite formation, austenite reversion, and athermal α′-formation, J. Magn. Magn. Mater. 473 (2019) 109–118, https://doi.org/10.1016/j.jmmm.2018.10.034.
[30] V. Shrinivas, S.K. Varma, L.E. Murr, Deformation-induced martensitic characteristics in 304 and 316 stainless steels during room-temperature rolling, Metall. Mater. Trans. A 26 (1995) 661–671, https://doi.org/10.1007/BF02663916.
[31] Y.F. Shen, X.X. Li, X. Sun, Y.D. Wang, L. Zuo, Twinning and martensite in a 304 austenitic stainless steel, Mater. Sci. Eng. A 552 (2012) 514–522, https://doi.org/10.1016/j.msea.2012.05.080.
[32] V. Seetharaman, R. Krishnan, Influence of the martensitic transformation on the deformation behaviour of an AISI 316 stainless steel at low temperatures, J. Mater. Sci. 16 (1981) 523–530, https://doi.org/10.1007/BF00738646.
[33] D.Y. Ryoo, N. Kang, C.Y. Kang, Effect of Ni content on the tensile properties and strain-induced martensite transformation for 304 stainless steel, Mater. Sci. Eng. A 528 (2011) 2277–2281, https://doi.org/10.1016/j.msea.2010.12.022.
[34] A. Rezaee, A. Kermanpur, A. Najafizadeh, M. Moallemi, H. Samaei Baghbadorani, Investigation of cold rolling variables on the formation of strain-induced

martensite in 201L stainless steel, Mater. Des. 46 (2013) 49–53, https://doi.org/10.1016/j.matdes.2012.09.054.
[35] B. Petit, N. Gey, M. Cherkaoui, B. Bolle, M. Humbert, Deformation behavior and microstructure/texture evolution of an annealed 304 AISI stainless steel sheet. Experimental and micromechanical modeling, Int. J. Plast. 23 (2007) 323–341, https://doi.org/10.1016/j.ijplas.2006.07.002.
[36] M. Okayasu, H. Fukui, H. Ohfuji, T. Shiraishi, Strain induced martensite formation characteristics of austenite stainless steel during various loading conditions, Mater. Sci. Technol. (United Kingdom) 30 (2014) 301–308, https://doi.org/10.1179/1743284713Y.0000000353.
[37] M. Odnobokova, A. Belyakov, R. Kaibyshev, Grain refinement and strengthening of austenitic stainless steels during large strain cold rolling, Philos. Mag. 99 (2019) 531–556, https://doi.org/10.1080/14786435.2018.1546961.
[38] M. Odnobokova, A. Belyakov, R. Kaibyshev, Effect of severe cold or warm deformation on microstructure evolution and tensile behavior of a 316L stainless steel, Adv. Eng. Mater. 17 (2015) 1812–1820, https://doi.org/10.1002/adem.201500100.
[39] L.E. Murr, K.P. Staudhammer, S.S. Hecker, Effects of strain state and strain rate on deformation-induced transformation in 304 stainless steel: part II. microstructural study, Metall. Trans. A 13 (1982) 627–635, https://doi.org/10.1007/BF02644428.
[40] K. Mumtaz, S. Takahashi, J. Echigoya, Y. Kamada, L. Zhang, H. Kikuchi, K. Ara, M. Sato, Magnetic measurements of the reverse martensite to austenite transformation in a rolled austenitic stainless steel, J. Mater. Sci. 39 (2004) 1997–2010, https://doi.org/10.1023/B:JMSC.0000017761.64839.fc.
[41] D. Xu, X. Wan, J. Yu, G. Xu, G. Li, Effect of cold deformation on microstructures and mechanical properties of austenitic stainless steel, Metals (Basel) 8 (2018) 1–14, https://doi.org/10.3390/met8070522.
[42] V. Mertinger, E. Nagy, F. Tranta, J. Sólyom, Strain-induced martensitic transformation in textured austenitic stainless steels, Mater. Sci. Eng. A 481–482 (2008) 718–722, https://doi.org/10.1016/j.msea.2007.02.165.
[43] T. Masumura, N. Nakada, T. Tsuchiyama, S. Takaki, T. Koyano, K. Adachi, The difference in thermal and mechanical stabilities of austenite between carbon- and nitrogen-added metastable austenitic stainless steels, Acta Mater. 84 (2015) 330–338, https://doi.org/10.1016/j.actamat.2014.10.041.
[44] J. Manjanna, S. Kobayashi, Y. Kamada, S. Takahashi, H. Kikuchi, Martensitic transformation in SUS 316LN austenitic stainless steel at RT, J. Mater. Sci. 43 (2008) 2659–2665, https://doi.org/10.1007/s10853-008-2494-4.
[45] M. Mahmoudiniya, S. Kheirandish, M. Asadiasadabad, The effect of cold rolling on microstructure and mechanical properties of a new Cr–Mn austenitic stainless steel in comparison with AISI 316 stainless steel, Trans. Indian Inst. Met. 70 (2017) 1251–1259, https://doi.org/10.1007/s12666-016-0921-9.
[46] J. Lv, H. Luo, Effects of strain and strain-induced α′-martensite on passive films in AISI 304 austenitic stainless steel, Mater. Sci. Eng. C 34 (2014) 484–490, https://doi.org/10.1016/j.msec.2013.10.003.
[47] J.A. Lichtenfeld, M.C. Mataya, C.J. Van Tyne, Effect of strain rate on stress-strain behavior of alloy 309 and 304L austenitic stainless steel, Metall. Mater. Trans. A Phys. Metall. Mater. Sci. 37 (2006) 147–161, https://doi.org/10.1007/s11661-006-0160-5.
[48] X. Li, Y. Wei, Z. Wei, J. Zhou, Effect of cold rolling on microstructure and mechanical properties of AISI 304N stainless steel, IOP Conf. Ser. Earth Environ. Sci. 252 (2019), https://doi.org/10.1088/1755-1315/252/2/022027.
[49] A.A. Lebedev, V.V. Kosarchuk, Influence of phase transformations on the mechanical properties of austenitic stainless steels, Int. J. Plast. 16 (2000) 749–767, https://doi.org/10.1016/S0749-6419(99)00085-6.
[50] B. Kuhfuss, E. Moumi, B. Clausen, J. Epp, B. Koehler, Investigation of deformation induced martensitic transformation during incremental forming of 304 stainless steel wires, Key Eng. Mater. 651–653 (2015) 645–650, https://doi.org/10.4028/www.scientific.net/KEM.651-653.645.
[51] R. Kreethi, P. Sampark, G.K. Majhi, K. Dutta, Martensitic transformation during compressive deformation of a non-conventional stainless steel and its quantitative assessment, J. Mater. Eng. Perform. 24 (2015) 4219–4223, https://doi.org/10.1007/s11665-015-1724-6.
[52] A. Kisko, R.D.K. Misra, J. Talonen, L.P. Karjalainen, The influence of grain size on the strain-induced martensite formation in tensile straining of an austenitic 15Cr-9Mn-Ni-Cu stainless steel, Mater. Sci. Eng. A 578 (2013) 408–416, https://doi.org/10.1016/j.msea.2013.04.107.
[53] J.M. Pardal, S.S.M. Tavares, M.T. Tavares, P.S.P. Garcia, J.A.C. Velasco, H.F. G. Abreu, J.P. Pardal, Influence of carbon content on the martensitic transformation of titanium stabilized austenitic stainless steels, Int. J. Adv. Manuf. Technol. 108 (2020) 345–356, https://doi.org/10.1007/s00170-020-05138-8.
[54] G.L. Huang, D.K. Matlock, G. Krauss, Martensite formation, strain rate sensitivity, and deformation behavior of type 304 stainless steel sheet, Metall. Trans. A Phys. Metall. Mater. Sci. 20 A (1989) 1239–1246, https://doi.org/10.1007/BF02647406.
[55] J. He, F. Yuan, M. Yang, L. Zhou, S. Jiao, X. Wu, Exceptional tensile properties under cryogenic temperature in heterogeneous laminates induced by non-uniform martensite transformation and strain delocalization, Mater. Sci. Eng. A 791 (2020) 139780, https://doi.org/10.1016/j.msea.2020.139780.
[56] P. Haušild, V. Davydov, J. Drahokoupil, M. Landa, P. Pilvin, Characterization of strain-induced martensitic transformation in a metastable austenitic stainless steel, Mater. Des. 31 (2010) 1821–1827, https://doi.org/10.1016/j.matdes.2009.11.008.
[57] H.N. Han, C.G. Lee, C.S. Oh, T.H. Lee, S.J. Kim, A model for deformation behavior and mechanically induced martensitic transformation of metastable austenitic steel, Acta Mater. 52 (2004) 5203–5214, https://doi.org/10.1016/j.actamat.2004.07.031.
[58] L.C.M. Gilapa, C.A.S. de Oliveira, M.R. da Silva, Effect of copper on the formation of strain-induced martensite in two austenitic stainless steels AISI 304, Mater. Sci. Eng. A 622 (2015) 212–218, https://doi.org/10.1016/j.msea.2014.10.059.
[59] C. Gauss, I.R. Souza Filho, M.J.R. Sandim, P.A. Suzuki, A.J. Ramirez, H.R. Z. Sandim, In situ synchrotron X-ray evaluation of strain-induced martensite in AISI 201 austenitic stainless steel during tensile testing, Mater. Sci. Eng. A 651 (2016) 507–516, https://doi.org/10.1016/j.msea.2015.10.110.
[60] M. Eskandari, A. Najafizadeh, A. Kermanpur, Effect of strain-induced martensite on the formation of nanocrystalline 316L stainless steel after cold rolling and annealing, Mater. Sci. Eng. A 519 (2009) 46–50, https://doi.org/10.1016/j.msea.2009.04.038.
[61] M. El-Tahawy, P. Jenei, T. Kolonits, G. Han, H. Park, H. Choe, J. Gubicza, Different evolutions of the microstructure, texture, and mechanical performance during tension and compression of 316L stainless steel, Metall. Mater. Trans. A Phys. Metall. Mater. Sci. 51 (2020) 3447–3460, https://doi.org/10.1007/s11661-020-05782-5.
[62] E.A. Eid, M.M. Sadawy, Role of effective strain during cold rolling deformation on mechanical characteristics of AISI 304 steel, Met. Mater. Int. (2020), https://doi.org/10.1007/s12540-020-00722-9.
[63] A.K. De, J.G. Speer, D.K. Matlock, D.C. Murdock, M.C. Mataya, R.J. Comstock, Deformation-induced phase transformation and strain hardening in type 304 austenitic stainless steel, Metall. Mater. Trans. A Phys. Metall. Mater. Sci. 37 (2006) 1875–1886, https://doi.org/10.1007/s11661-006-0130-y.
[64] Y.B. Das, A.N. Forsey, J. Kelleher, S. Kabra, M.E. Fitzpatrick, T.H. Simm, S. Gungor, R.J. Moat, The influence of temperature on deformation-induced martensitic transformation in 301 stainless steel, Mater. Sci. Technol. (United Kingdom) 34 (2018) 2114–2125, https://doi.org/10.1080/02670836.2018.1511076.
[65] J.Y. Choi, W. Jin, Strain induced martensite formation and its effect on strain hardening behavior in the cold drawn 304 austenitic stainless steels, Scr. Mater. 36 (1997) 99–104, https://doi.org/10.1016/S1359-6462(96)00338-7.
[66] C. Celada-Casero, H. Kooiker, M. Groen, J. Post, D. San-Martin, In-situ investigation of strain-induced martensitic transformation kinetics in an austenitic stainless steel by inductive measurements, Metals (Basel) 7 (2017), https://doi.org/10.3390/met7070271.
[67] M. Bigdeli Karimi, H. Arabi, A. Khosravani, J. Samei, Effect of rolling strain on transformation induced plasticity of austenite to martensite in a high-alloy austenitic steel, J. Mater. Process. Technol. 203 (2008) 349–354, https://doi.org/10.1016/j.jmatprotec.2007.10.029.
[68] F. Abedi, S. Serajzadeh, Mechanical properties and strain-induced martensite transformation in cold rolling of 304L stainless steel plate, J. Mater. Eng. Perform. 27 (2018) 6155–6165, https://doi.org/10.1007/s11665-018-3643-9.
[69] J.M. Alves, L.P. Brandão, A. Dos, Santos Paula, Mechanically induced martensitic transformation of hot rolled and annealed 304L austenitic stainless steel at room and cryogenic temperatures, Mater. Res. 22 (2019) 6–10, https://doi.org/10.1590/1980-5373-MR-2019-0150.
[70] N. Solomon, I. Solomon, Deformation induced martensite in AISI 316 stainless steel, Rev. Metal. 46 (2010) 121–128, https://doi.org/10.3989/revmetalm.0920.
[71] S. Nanga, A. Pineau, B. Tanguy, P.O. Santacreu, Strain induced martensitic transformations in two austenitic stainless steels: Macro-micro behaviour, 17th Eur. Conf. Fract. 2008 Multilevel Approach to Fract. Mater. Components Struct. 2 (2008) 1373–1380.
[72] O.P. Maksimkin, Deformation induced martensitic transformation in Cr-Ni stainless steel irradiated by neutrons, Phys. Status Solidi Appl. Res. 163 (1997), https://doi.org/10.1002/1521-396X(199709)163:1<R7::AID-PSSA99997>3.0.CO;2-T.
[73] A.K. De, D.C. Murdock, M.C. Mataya, J.G. Speer, D.K. Matlock, Quantitative measurement of deformation-induced martensite in 304 stainless steel by X-ray diffraction, Scr. Mater. 50 (2004) 1445–1449, https://doi.org/10.1016/j.scriptamat.2004.03.011.
[74] A. Kanni Raj, K.A. Padmanabhan, Room-temperature plastic flow and strain-induced martensitic transformation in 1.2 wt% Ni metastable austenitic stainless steel sheets, J. Mater. Sci. Lett. 16 (1997) 1920–1924, https://doi.org/10.1023/A:1018534616852.
[75] V. Talyan, R.H. Wagoner, J.K. Lee, Formability of stainless steel, Metall. Mater. Trans. A Phys. Metall. Mater. Sci. 29 (1998) 2161–2172, https://doi.org/10.1007/s11661-998-0041-1.
[76] Y. Matsuoka, T. Iwasaki, N. Nakada, T. Tsuchiyama, S. Takaki, Effect of grain size on thermal and mechanical stability of austenite in metastable austenitic stainless steel, ISIJ Int. 53 (2013) 1224–1230, https://doi.org/10.2355/isijinternational.53.1224.
[77] C. Zheng, H. Jiang, X. Hao, J. Ye, L. Li, D. Li, Tailoring mechanical behavior of a fine-grained metastable austenitic stainless steel by pre-straining, Mater. Sci. Eng. A 746 (2019) 332–340, https://doi.org/10.1016/J.MSEA.2019.01.038.
[78] F. Peng, X. Dong, K. Liu, H. Xie, Effects of strain rate and plastic work on martensitic transformation kinetics of austenitic stainless steel 304, J. Iron Steel Res. Int. 22 (2015) 931–936, https://doi.org/10.1016/S1006-706X(15)30092-3.
[79] U. Krupp, C. West, H.J. Christ, Deformation-induced martensite formation during cyclic deformation of metastable austenitic steel: influence of temperature and carbon content, Mater. Sci. Eng. A 481–482 (2008) 713–717, https://doi.org/10.1016/J.MSEA.2006.12.211.
[80] Y.-S. Jung, Y.-K. Lee, D.K. Matlock, M.C. Mataya, Effect of grain size on strain-induced martensitic transformation start temperature in an ultrafine grained metastable austenitic steel, Met. Mater. Int. 17 (2011) 553–556, https://doi.org/10.1007/s12540-011-0804-x.
[81] D. Fahr, Stress- and strain-induced formation of martensite and its effects on strength and ductility of metastable austenitic stainless steels, Metall. Trans. 2 (1971) 1883–1892, https://doi.org/10.1007/BF02913420.

[82] A. Das, S. Sivaprasad, P.C. Chakraborti, S. Tarafder, Morphologies and characteristics of deformation induced martensite during low cycle fatigue behaviour of austenitic stainless steel, Mater. Sci. Eng. A 528 (2011) 7909–7914, https://doi.org/10.1016/J.MSEA.2011.07.011.
[83] M. Waskom, Seaborn: Statistical Data Visualization, J. Open Source Softw. 6 (2021) 3021, https://doi.org/10.21105/joss.03021.
[84] D. Genève, D. Rouxel, P. Pigeat, M. Confente, Descaling ability of low-alloy steel wires depending on composition and rolling process, Corros. Sci. 52 (2010) 1155–1166, https://doi.org/10.1016/J.CORSCI.2009.12.028.
[85] X. Ying, An Overview of Overfitting and its Solutions, J. Phys. Conf. Ser. 1168 (2019) 22022, https://doi.org/10.1088/1742-6596/1168/2/022022.
[86] A. Pasini, Artificial neural networks for small dataset analysis, J. Thorac. Dis. 7 (2015) 953–960, https://doi.org/10.3978/j.issn.2072-1439.2015.04.61.
[87] S. ichi Amari, Backpropagation and stochastic gradient descent method, Neurocomputing 5 (1993) 185–196, https://doi.org/10.1016/0925-2312(93)90006-O.
[88] A. Paszke, S. Gross, F. Massa, A. Lerer, J. Bradbury, G. Chanan, T. Killeen, Z. Lin, N. Gimelshein, L. Antiga, A. Desmaison, A. Köpf, E. Yang, Z. DeVito, M. Raison, A. Tejani, S. Chilamkurthy, B. Steiner, L. Fang, J. Bai, S. Chintala, PyTorch: an imperative style, high-performance deep learning library, Adv. Neural Inf. Process. Syst. 32 (2019).
[89] J.D. Hunter, Matplotlib: a 2D graphics environment, Comput. Sci. Eng. 9 (2007) 90–95, https://doi.org/10.1109/MCSE.2007.55.
[90] A. Järvenpää, M. Jaskari, J. Man, L.P. Karjalainen, Austenite stability in reversion-treated structures of a 301LN steel under tensile loading, Mater. Charact. 127 (2017) 12–26, https://doi.org/10.1016/j.matchar.2017.01.040.
[91] D. Maréchal, Linkage between mechanical properties and phase transformations in a 301LN austenitic stainless steel, (2011). ⟨https://open.library.ubc.ca/collections/24/items/1.0071814⟩.
[92] A. Saeed-Akbari, J. Imlau, U. Prahl, W. Bleck, Derivation and variation in composition-dependent stacking fault energy maps based on subregular solution model in high-manganese steels, Metall. Mater. Trans. A 40 (2009) 3076–3090, https://doi.org/10.1007/s11661-009-0050-8.
[93] M.C. Somani, P. Juntunen, L.P. Karjalainen, R.D.K. Misra, A. Kyröläinen, Enhanced mechanical properties through reversion in metastable austenitic stainless steels, Metall. Mater. Trans. A 40 (2009) 729–744, https://doi.org/10.1007/s11661-008-9723-y.
[94] A. Jain, A. Varshney, A critical review on deformation-induced transformation kinetics of austenitic stainless steels, Mater. Sci. Technol. 0 (n.d.) 02670836231212618. https://doi.org/10.1177/02670836231212618.
[95] J. Talonen, H. Hänninen, P. Nenonen, G. Pape, Effect of strain rate on the strain-induced $\gamma \rightarrow \alpha'$-martensite transformation and mechanical properties of austenitic stainless steels, Metall. Mater. Trans. A 36 (2005) 421–432, https://doi.org/10.1007/s11661-005-0313-y.
[96] P.J. Ferreira, J.B. Vander Sande, M.A. Fortes, A. Kyrolainen, Microstructure development during high-velocity deformation, Metall. Mater. Trans. A 35 (2004) 3091–3101, https://doi.org/10.1007/s11661-004-0054-3.
[97] D. Montes de Oca Zapiain, J.A. Stewart, R. Dingreville, Accelerating phase-field-based microstructure evolution predictions via surrogate models trained by machine learning methods, Npj Comput. Mater. 7 (2021) 3, https://doi.org/10.1038/s41524-020-00471-8.
[98] A. Kumar Thakur, S. Kovacevic, V.R. Manga, P.A. Deymier, K. Muralidharan, A first-principles and CALPHAD-assisted phase-field model for microstructure evolution: application to Mo-V binary alloy systems, Mater. Des. (2023) 112443, https://doi.org/10.1016/J.MATDES.2023.112443.